JCI The Journal of Clinical Investigation

NO triggers RGS4 degradation to coordinate angiogenesis and cardiomyocyte growth

Irina M. Jaba, … , Lawrence H. Young, Daniela Tirziu

J Clin Invest. 2013;123(4):1718-1731. https://doi.org/10.1172/JCI65112.

Research Article **Cardiology**

Myocardial hypertrophy is an adaptation to increased hemodynamic demands. An increase in heart tissue must be matched by a corresponding expansion of the coronary vasculature to maintain and adequate supply of oxygen and nutrients for the heart. The physiological mechanisms that underlie the coordination of angiogenesis and cardiomyocyte growth are unknown. We report that induction of myocardial angiogenesis promotes cardiomyocyte growth and cardiac hypertrophy through a novel NO-dependent mechanism. We used transgenic, conditional overexpression of placental growth factor (PlGF) in murine cardiac tissues to stimulate myocardial angiogenesis and increase endothelial-derived NO release. NO production, in turn, induced myocardial hypertrophy by promoting proteasomal degradation of regulator of G protein signaling type 4 (RGS4), thus relieving the repression of the Gβγ/PI3Kγ/AKT/mTORC1 pathway that stimulates cardiomyocyte growth. This hypertrophic response was prevented by concomitant transgenic expression of RGS4 in cardiomyocytes. NOS inhibitor L-NAME also significantly attenuated RGS4 degradation, and reduced activation of AKT/mTORC1 signaling and induction of myocardial hypertrophy in PlGF transgenic mice, while conditional cardiac-specific PlGF expression in eNOS knockout mice did not induce myocardial hypertrophy. These findings describe a novel NO/RGS4/Gβγ/PI3Kγ/AKT mechanism that couples cardiac vessel growth with myocyte growth and heart size.

NO triggers RGS4 degradation to coordinate angiogenesis and cardiomyocyte growth

Irina M. Jaba,[1] Zhen W. Zhuang,[1] Na Li,[1] Yifeng Jiang,[2] Kathleen A. Martin,[1,3] Albert J. Sinusas,[1,2] Xenophon Papademetris,[4] Michael Simons,[1,5] William C. Sessa,[3] Lawrence H. Young,[1,6] and Daniela Tirziu[1]

[1]Yale Cardiovascular Research Center, Section of Cardiovascular Medicine, Department of Internal Medicine, [2]Department of Diagnostic Radiology, [3]Department of Pharmacology, [4]Departments of Diagnostic Radiology and Biomedical Engineering, [5]Department of Cell Biology, and [6]Department of Molecular Physiology, Yale School of Medicine, New Haven, Connecticut, USA.

Myocardial hypertrophy is an adaptation to increased hemodynamic demands. An increase in heart tissue must be matched by a corresponding expansion of the coronary vasculature to maintain and adequate supply of oxygen and nutrients for the heart. The physiological mechanisms that underlie the coordination of angiogenesis and cardiomyocyte growth are unknown. We report that induction of myocardial angiogenesis promotes cardiomyocyte growth and cardiac hypertrophy through a novel NO-dependent mechanism. We used transgenic, conditional overexpression of placental growth factor (PlGF) in murine cardiac tissues to stimulate myocardial angiogenesis and increase endothelial-derived NO release. NO production, in turn, induced myocardial hypertrophy by promoting proteasomal degradation of regulator of G protein signaling type 4 (RGS4), thus relieving the repression of the Gβγ/PI3Kγ/AKT/mTORC1 pathway that stimulates cardiomyocyte growth. This hypertrophic response was prevented by concomitant transgenic expression of RGS4 in cardiomyocytes. NOS inhibitor L-NAME also significantly attenuated RGS4 degradation, and reduced activation of AKT/mTORC1 signaling and induction of myocardial hypertrophy in PlGF transgenic mice, while conditional cardiac-specific PlGF expression in eNOS knockout mice did not induce myocardial hypertrophy. These findings describe a novel NO/RGS4/Gβγ/PI3Kγ/AKT mechanism that couples cardiac vessel growth with myocyte growth and heart size.

Introduction

Recent studies have increased appreciation for the relationship between cardiomyocyte growth and angiogenesis and its contribution to molecular regulation of the myocardial hypertrophic response. Myocardial hypertrophy, secondary to increased hemodynamic demands, requires commensurate growth of the coronary vasculature to provide adequate oxygen and nutrients to the increasing cardiac mass; lack of coordination between the myocyte-driven hypertrophic response and the production of angiogenic growth factors hallmarks the transition to heart failure (1). Although vascular endothelium controls a plethora of biological events contributing to cardiovascular homeostasis, including regulation of vascular tone, thrombosis, and myocardial stiffness, little is known about the effect of endothelial signaling on cardiomyocyte growth, regulation of myocardial hypertrophy, and heart size. Our previous observation that a NOS inhibitor, N^G-nitro-L-arginine methyl ester (L-NAME), partially prevented angiogenesis-driven myocardial hypertrophy (2) suggests that endothelium-dependent NO production might be responsible for the hypertrophic effect on cardiomyocytes and the increase in heart size.

Because there are no known mechanisms that link NO to stimulation of cardiomyocyte hypertrophy, we designed the present study to fill this gap. In cardiomyocytes, G protein–mediated hypertrophic signaling is negatively modulated by regulators of G protein signaling (RGS proteins). Among more than 20 RGS proteins, RGS subtype 4, a GTPase-activating protein for heterotrimeric Gq and Gi (3), is associated with regulation of the hypertrophic response in failing human myocardium (4, 5). RGS4 bears an N-terminal Cys residue that is targeted for ubiquitin-dependent degradation by arginylation through the Arg/N-end rule pathway of protein degradation (6, 7). Since NO controls N-terminal Cys oxidation prior to its arginylation and, ultimately, the rate at which proteins are degraded through the Arg/N-end rule pathway (8), we explored whether NO-mediated RGS4 degradation can account for angiogenesis-driven myocyte hypertrophy. The G protein heterotrimer consists of a Gα subunit that in its GDP-bound transition state is tightly associated with an obligate Gβγ dimer. RGS4 negatively regulates G protein activation by accelerating GTP hydrolysis of the GTP-bound Gα subunit and stabilizes the transition state, and/or by competing for G protein binding to effectors (9–11). Hypertrophic signaling through Gq is mediated downstream of the Gαq subunit via several pathways, including calcineurin/nuclear factor of activated T cells (calcineurin/NFAT), PKC, and MAPKs (12–15). Among the downstream effectors of Gβγ subunits, PI3K p110γ is of particular interest, because of its role in v-akt murine thymoma viral proto-oncogene 1 (Akt) activation that ultimately mediates myocyte hypertrophy through the mammalian target of rapamycin complex 1 (mTORC1) pathway (16–19).

We hypothesized that an increase in vascular endothelium in the adult heart increases NO production, which in turn drives cardiomyocyte growth by accelerating RGS4 degradation and activating G protein signaling. Consequently, if increased NO production favors a loss of RGS4 function, then increased RGS4 expression should compensate for this and prevent hypertrophic stimulation.

In order to induce myocardial angiogenesis, we chose placental growth factor (PlGF), a more targeted angiogenic factor than PR39, which we used in our previous report (2). A member of the VEGF

Conflict of interest: The authors have declared that no conflict of interest exists.
Citation for this article: *J Clin Invest.* 2013;123(4):1718–1731. doi:10.1172/JCI65112.

family, PlGF binds VEGFR1 (also known as Flt1) and indirectly amplifies the angiogenic response to VEGF-A by displacing VEGF-A from VEGFR1 and making it available for binding to VEGFR2 (also known as Flk1) (20, 21). Previous studies have shown that PlGF promotes collateral growth and improves perfusion after femoral artery ligation (22, 23). In pathological settings of myocardial infarct or pressure overload, PlGF stimulates angiogenesis and fibroblast proliferation that, in turn, may support cardiomyocyte hypertrophy through a paracrine mechanism (24, 25).

Here, we designed cardiac-specific inducible doxycycline withdrawal mouse models to (a) selectively stimulate myocardial angiogenesis by PlGF, (b) stimulate angiogenesis by PlGF and compensate for RGS4 degradation by transgenic expression of RGS4 in cardiomyocytes, and (c) stimulate angiogenesis in *eNOS* gene knockout. Using conditional mouse models and cell culture systems, we showed that increased NO production subsequent to angiogenic stimulation in the heart resulted in RGS4 degradation that released Gβγ inhibition and induced hypertrophic signaling, at least in part, through the Akt/mTORC1 pathway. This novel NO/RGS4/G protein/Akt mechanism triggered hypertrophic signaling in cardiomyocytes in the absence of traditional hypertrophic stimuli, and it may be a fundamental mechanism that coordinates vessel growth with myocyte growth in adult heart.

Results

RGS4 gain of function prevents myocardial hypertrophy subsequent to angiogenic stimulation in heart and increased NO release. Inducible cardiac-specific expression of *PlGF* or concomitantly induced cardiac-expression of *PlGF* and *RGS4* were achieved using a bidirectional tetracycline response element (*TRE*) regulated by a tetracycline transactivator (*tTA*) driven by α–myosin heavy chain (α*MHC*) promoter (Supplemental Figure 1A; supplemental material available online with this article; doi:10.1172/JCI65112DS1). Doxycycline withdrawal–driven expression of *TRE-PlGF/LacZ* or *TRE-PlGF/RGS4* was initially confirmed in MEF/3T3 cells stably expressing *tTA* (Supplemental Figure 1B). We subsequently generated *PlGF*- and *PlGF/RGS4*-inducible mice (referred to herein as PlGF and PlGF/RGS4 mice, respectively) by crossing newly generated *TRE-PlGF/LacZ* and *TRE-PlGF/RGS4* responder mouse lines with driver line α*MHC-tTA*. As determined by real-time PCR–based genotyping, PlGF and PlGF/RGS4 mice showed relatively equal transgene copy numbers (Supplemental Figure 1C). The transgenes were then induced in 5-week-old mice for 3 weeks and 6 weeks, in the absence of doxycycline (Tet-OFF) (Supplemental Figure 1, D–G). The presence of doxycycline (Tet-ON) in PlGF mice during the 6-week stimulation period — used as a negative control for transgene expression — did not result in cardiac hypertrophy (Supplemental Figure 1, H and I).

In order to determine the relationship between angiogenic stimulation and myocardial hypertrophy onset, we analyzed hearts after 3 and 6 weeks of transgene induction. There was a significant increase of the capillary/myocyte ratio, from 1 in controls to approximately 1.5 in PlGF and PlGF/RGS4 mice, at both 3 and 6 weeks (Figure 1, A and B). After 6 weeks of angiogenic stimulation, we examined cardiac vasculature using high-resolution micro-CT to visualize the hearts after casting with a bismuth-based contrast agent (Supplemental Figure 2A). Quantitative analysis of the vasculature extracted from the resulting micro-CT angiograms showed a significant increase in arteriolar branches greater than 24 μm and up to 96 μm in diameter in both PlGF and PlGF/RGS4 mice compared with controls (Figure 1C), which were homogenously distributed throughout the myocardium (Supplemental Figure 2B). Furthermore, a 3D morphometric analysis, based on a computational reconstruction of the arteriolar tree, demonstrated an increase in distal branching in both conditional mouse models. As shown in Figure 1, D and E, there was a significant increase in arterial branches (28–72 μm in diameter), with higher branching levels — ranging 30–80 — in PlGF and PlGF/RGS4 mice compared with controls. This correlated well with the increased number of short branches (up to 400 μm in vessel length; Figure 1F).

To determine whether the increased coronary vasculature leads to increased NO release, we assessed the activity of protein kinases dependent on cGMP (PKG) as readout for NO production. Although there was no significant change in PKG activity at 3 weeks, activity at 6 weeks increased approximately 2-fold in both PlGF and PlGF/RGS4 mice (Figure 2A). To determine whether eNOS is the source of NO, LV myocardium cross-sections were immunostained with anti-eNOS Ab. Consistent with the angiogenic stimulation, eNOS expression in the endothelium at 6 weeks was approximately 2.5-fold higher in both inducible models than in control mice (Figure 2, B and C). Because eNOS expression in tissue sections was mostly associated with endothelium, the eNOS level in cardiomyocytes was determined by Western blotting using protein lysates from freshly isolated cardiomyocytes. Our data showed roughly equal eNOS expression in cardiomyocytes in PlGF, PlGF/RGS4, and control mice at 6 weeks (Figure 2D). There was also no apparent increase in neuronal NOS (nNOS) or iNOS expression in isolated cardiomyocytes between groups at the same time (Figure 2D). These data indicate that endothelial eNOS is the source of NO production.

Next, we assessed cardiac hypertrophy subsequent to myocardial angiogenesis and increased NO production. After 3 weeks, there was no significant difference in heart size (Figure 3A). However, after 6 weeks, there was up to a 50% increase in heart weight/body weight ratio in PlGF mice, but less hypertrophy in PlGF/RGS4 mice (Figure 3A). The increased heart size in PlGF mice at 6 weeks was associated with a loss of RGS4, whereas *RGS4* transgene expression in the PlGF/RGS4 model restored RGS4 protein to normal levels and prevented the hypertrophic effect (Figure 3B). These results are consistent with our hypothesis that an increase in vascular endothelium results in an increase in NO production that triggers RGS4 degradation. Consequently, an increase in RGS4 expression stabilizes the protein level and attenuates the hypertrophic signaling. Similar to our previously reported PR39 model (2), the angiogenesis induced at 3 weeks preceded the 46% increase in cardiomyocyte size measured at 6 weeks in LV myocardium cross-sections or isolated cardiomyocytes (Figure 3, C and D). The increase in myocyte surface area was mostly due to increased cell thickness, rather than increased cell length (Supplemental Figure 3). Despite similar capillary/myocyte ratios and NO release (based on PKG activity), myocyte size in PlGF/RGS4 mice was reduced by 80% compared with PlGF mice (Figure 3, C and D), in agreement with the reduced heart weight/body weight ratio (Figure 3A).

To further characterize cardiac morphology and function, we performed M-mode echocardiograms. In agreement with the histological observations, after 6 weeks of induction, there was a significant increase in LV wall thickness and mass in PlGF mice compared with controls (Figure 4, A and B). LV wall thickness and mass were significantly reduced in PlGF/RGS4 versus PlGF mice (Figure 4B). However, there was only a slight increase in LV

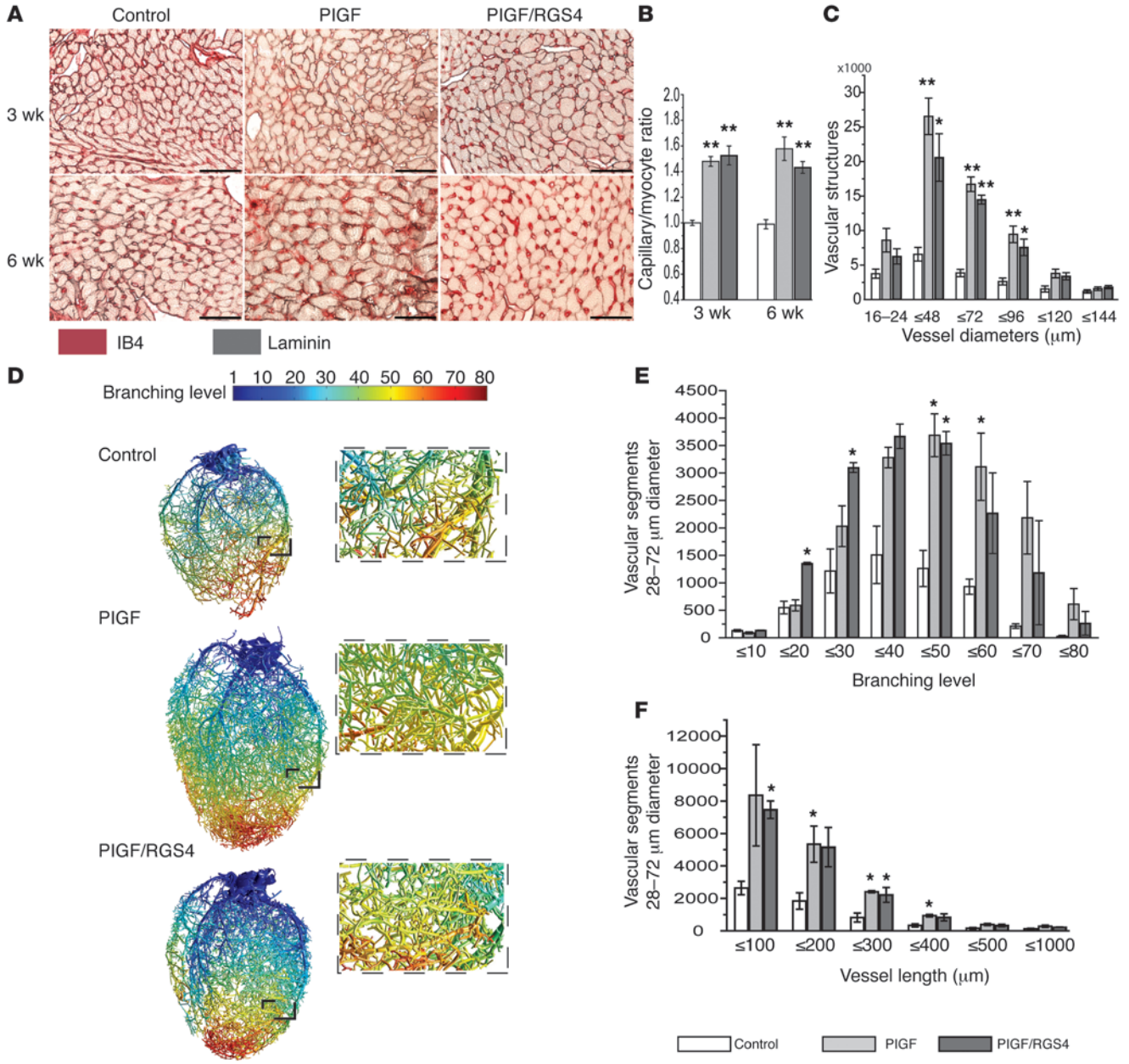

Figure 1

PlGF-induced increase of capillary density and arteriolar branching. (**A**) Representative immunostaining with anti-laminin Ab and IB4 staining of LV myocardium after 3 and 6 weeks of PlGF or PlGF/RGS4 transgene expression. Scale bars: 50 μm. (**B**) Capillary/myocyte ratio at 3 and 6 weeks in PlGF and PlGF/RGS4 mice compared with controls. (**C**) Quantitative assessment of the cardiac vasculature, extracted from micro-CT angiograms after 6 weeks of PlGF or PlGF/RGS4 transgene expression. Data represent total number of vascular structures of specified diameters counted in whole heart. Note the significant increase in vascular structures >24 and ≤96 μm in diameter in PlGF and PlGF/RGS4 mice ($n = 3$ per group) compared with controls ($n = 4$). (**D**) 3D computational reconstruction of the arteriolar tree. Branching level is indicated by color, ranging from blue (level 1; arterial root) to red (level 80). (**E**) Histogram representation of branching level for vascular segments 28–72 μm in diameter. Note the growth of arterial tree through distal branching ranging from branching level 30 to 80 in PlGF and PlGF/RGS4 mice compared with controls. (**F**) Histogram representation of vessel length for vascular segments 28–72 μm in diameter. Data represent vascular structures/segments of specified diameters normalized to LV mass/body weight ratio. *$P < 0.05$, **$P < 0.01$ vs. control.

diastolic diameter and volume and no change in LV systolic volume in PlGF mice compared with PlGF/RGS4 or control mice. To exclude the possibility that PlGF expression increases blood pressure, which could potentially trigger a Gq-mediated hypertrophic response, we measured blood pressure in PlGF mice after 6 weeks of induction. However, we found no increase in either systolic or diastolic aortic pressure (measured with a 1.4-F micromanometer catheter; see Methods) in PlGF versus control mice (Figure 4C). These results indicate that myocardial hypertrophy in PlGF mice is not caused by LV pressure overload. The hypertrophic response

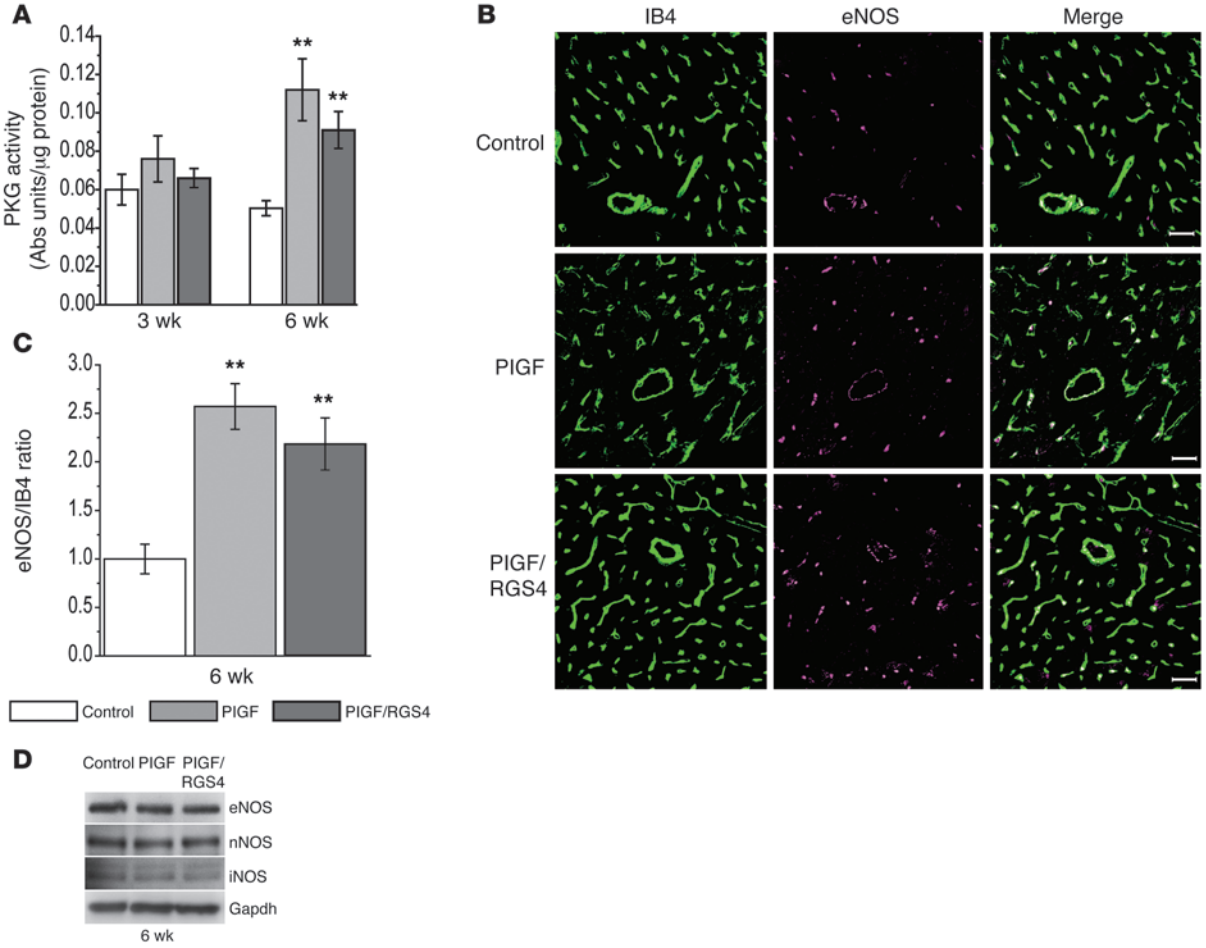

Figure 2

Increased endothelial-derived NO release. (**A**) PKG activity in LV tissue lysates after 3 and 6 weeks of transgene stimulation. Note the significant increase of PKG activity in PlGF and PlGF/RGS4 mice at 6 weeks. n = 8–14 per group. (**B**) Representative immunostaining, with anti-eNOS Ab and IB4, of LV myocardium cross-sections after 6 weeks of PlGF or PlGF/RGS4 transgene expression. Scale bars: 20 μm. (**C**) Quantification of eNOS expression in the endothelium at 6 weeks, determined as ratio of eNOS (red) to IB4 (green) staining. eNOS expression increased significantly in the endothelium in PlGF and PlGF/RGS4 mice compared with controls. (**D**) Expression level of eNOS, nNOS, and iNOS in freshly isolated cardiomyocytes after 6 weeks of PlGF or PlGF/RGS4 transgene expression (Western blotting). No increased expression of eNOS, nNOS, or iNOS was observed in cardiomyocytes in PlGF- or PlGF/RGS4 mice compared with controls. $^{**}P < 0.01$ vs. control.

to angiogenic stimulation was not a pathological one, as the LV ejection fraction was maintained in the normal range in both conditional models (Figure 4B). Furthermore, there was no discernible interstitial fibrosis (Figure 4D), which can accompany pathological hypertrophy.

PlGF has previously been reported to induce peripheral blood mononuclear cell recruitment into tissues (23). To determine whether inflammation plays a role in the hypertrophic response in our model, we looked for the presence of leukocytes in the myocardium in PlGF and PlGF/RGS4 mice. There was no recruitment of $CD45^+$ cells in the heart after 6 weeks of induction in PlGF and PlGF/RGS4 mice compared with controls (Supplemental Figure 4).

NO mediates cardiomyocyte growth through RGS4 degradation and activation of the Gβγ/PI3Kγ/Akt/mTORC1 pathway. In order to determine the molecular mechanism by which NO mediates cardiomyocyte growth, we first assessed the effect of the slow-acting NO donor DETA-NONOate (NO release $t_{1/2}$, 20 hours at 37°C) on cultured rat neonatal cardiomyocytes. Treatment of cultured myocytes with the NO donor significantly reduced RGS4 protein levels (Figure 5A). Consistent with NO mediating its effect through the Arg/N-end rule pathway, treatment with the proteasomal inhibitor MG132 prevented RGS4 degradation in cardiomyocytes exposed to the NO donor (Figure 5A). siRNA silencing of arginyltransferase 1 (*Ate1*), in order to inhibit arginylation of the N-terminal Cys in substrates, similarly prevented NO-induced degradation of RGS4 (Figure 5B).

We next determined whether RGS4 degradation in cardiomyocytes is sufficient to induce a hypertrophic signal. 24-hour treatment of cardiomyocytes with the NO donor induced a 70% increase in cell size compared with control, and this growth effect was 30% lower than that induced by the cardiac hypertrophic GPCR agonist Ang II (Figure 5, C and D). In contrast, PlGF treatment did not affect myocyte size, which suggests that the hypertrophy observed in vivo (Figures 3 and 4) is not due to a direct effect of PlGF on cardiomyocytes. The increase in cell size in NO donor–treated cardiomyocytes correlated with an approximately 3-fold increase in Akt^{Ser473}

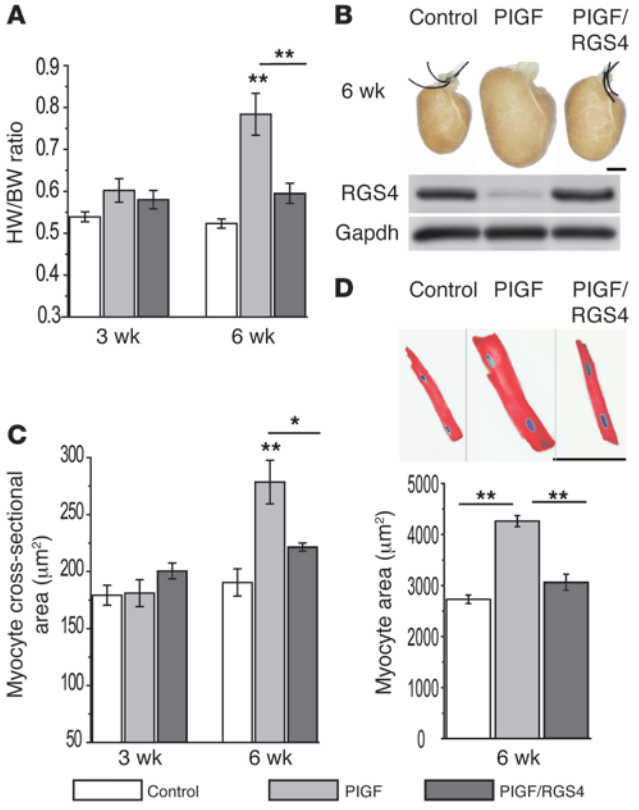

Figure 3
Cardiac hypertrophy subsequent to myocardial angiogenesis and increased NO release. (**A**) Heart weight/body weight ratio after 3 and 6 weeks of transgene expression. $n = 7$ (PlGF 3 wk); 8 (PlGF 6 wk and PlGF/RGS4 6 wk); 9 (PlGF/RGS4 3 wk); 18 (control 3 wk); 24 (control 6 wk). (**B**) Heart images after 6 weeks induction and RGS4 protein level in PlGF, PlGF/RGS4, and control mice. Scale bar: 2 mm. Note the loss of RGS4 in PlGF mice and restoration to normal level in PlGF/RGS4 mice. (**C**) Cardiomyocyte cross-sectional area in LV myocardium sections after 3 and 6 weeks induction of PlGF or PlGF/RGS4 transgene compared with controls. (**D**) Micrographs of isolated cardiomyocytes immunostained with anti–α-actinin sarcomeric Ab and DAPI and quantification of cardiomyocyte surface area after 6 weeks of transgene expression compared with controls. Scale bar: 100 μm. $^*P < 0.05$, $^{**}P < 0.01$ vs. control or as indicated by brackets.

phosphorylation (Figure 5E). Akt activation led to inhibition of its substrate, tuberous sclerosis 2 (Tsc2), by increasing $Tsc2^{Ser939}$ phosphorylation approximately 2-fold. This in turn resulted in activation of the mTORC1 pathway, as measured by increased phosphorylation of p70-$S6K^{Thr389}$ (Figure 5E). Notably, there was no Akt/mTORC1 pathway activation in PlGF-treated cardiomyocytes in culture (Figure 5, D and E), which further indicates that PlGF does not stimulate cardiomyocytes directly. After 24 hours, in Ang II–treated cells, there was modest and comparable activation of Akt^{Ser473} and $Tsc2^{Ser939}$ phosphorylation (1.5- and 1.3-fold increases, respectively). These minor changes in Akt activity have little relevance to its hypertrophic effect, and it is known that Ang II–induced Akt activation is transient, peaking in less than an hour (26).

Next, to determine whether NO controls RGS4 degradation and Akt activation in the condition of RGS4 overexpression, RGS4-expressing cardiomyocytes were exposed to the NO donor. Cardiomyocytes transfected with RGS4 plasmid expressed twice as much RGS4 protein as did control plasmid–transfected cells (Figure 5F). Although treatment with the NO donor reduced RGS4 expression, it only brought RGS4 content down to control levels. Since a drop to low RGS4 levels was effectively prevented, NO donor did not activate Akt in RGS4-overexpressing cells (Figure 5F). These findings indicate that RGS4 content needs to be reduced below control levels in order to relieve RGS4-mediated inhibition of the Akt pathway.

In order to determine whether downregulation of *RGS4* gene expression leads to Akt activation, we suppressed *RGS4* expression with siRNA. Indeed, reducing *RGS4* expression significantly increased Akt^{Ser473} phosphorylation that bolstered Akt kinase activity approximately 2-fold, as determined by an in vitro assay with GSK-3 as substrate (Figure 5G).

Finally, to determine whether Akt activation is induced by Gβγ-dependent PI3Kγ activation, we used a scavenger for Gβγ subunits, the carboxyterminal peptide of GPCR kinase 2 (GRK2-CT; also known as βARKct; ref. 27), a specific PI3Kγ inhibitor, AS605240 (28), and a pan-PI3K inhibitor, LY294002. In NO-treated cells, transduction with adenovirus encoding βARKct (Ad-βARKct) or treatment with AS605240 or LY294002 prevented Akt^{Ser473} phosphorylation (Figure 5, H and I). Together, these data suggest that the freely dissociated Gβγ subunits — due to RGS4 loss of function — activate PI3Kγ, which in turn mediates the hypertrophic signal through the Akt/mTORC1 pathway.

It is known that Ang II promotes pathological hypertrophy via Gαq-dependent activation of the calcineurin/NFAT pathway (29, 30). While NFAT was activated by Ang II, NO treatment did not stimulate NFAT promoter activity (Supplemental Figure 5). This finding demonstrates that the RGS4 loss of function in NO-treated cells is not sufficient to activate the NFAT hypertrophic signal. It is likely that the effect of NO is propagated by the Gβγ/Akt/mTORC1 pathway, as opposed to the Gαq/calcineurin/NFAT pathway.

RGS4 gain of function prevents Akt/mTORC1 activation subsequent to increased NO. Consistent with our in vitro findings indicative of a RGS4/Gβγ/PI3Kγ/Akt link (Figure 5), myocardial hypertrophy subsequent to angiogenic stimulation in PlGF mice was associated with reduced RGS4 protein level and Akt/mTORC1 pathway activation (Figure 3B and Figure 6A). To exclude the possibility that the loss of RGS4 protein in PlGF mice is caused by a decrease in gene expression, we next determined the level of *RGS4* mRNA expression, which was slightly increased at 3 weeks and similar to controls at 6 weeks (Figure 6B), suggesting that the loss in RGS4 was due to protein degradation. Myocardial hypertrophy in PlGF mice at 6 weeks was associated with a 1.7-fold increase in Akt^{Ser473} phosphorylation and a 3.5-fold increase in Akt kinase activity, determined in an in vitro assay using GSK-3 as substrate (Figure 6, A and C). Consistent with Akt activation in PlGF mice at 6 weeks, there was an approximately 3-fold increase in $Tsc2^{Ser939}$ phosphorylation and a 7-fold increase in p70-$S6K^{Thr389}$ phosphorylation (Figure 6A). At the same time, PlGF/RGS4 mice had blunted Akt activation and phosphorylation of Tsc2 and p70-S6K (Figure 6, A and C).

Furthermore, we assessed whether downstream pathways regulated by Ang II/Gq signaling are activated in PlGF mice. Specifically, we investigated whether activation of the MAPK/Erk and calcineurin/NFAT pathway increases; however, Western blot analysis of $Erk1/2^{Thr202/Tyr204}$ phosphorylation showed no activation in PlGF mice compared with controls after 3 and 6 weeks of induction (Figure 6, A and C). NFAT transcription factors are normally

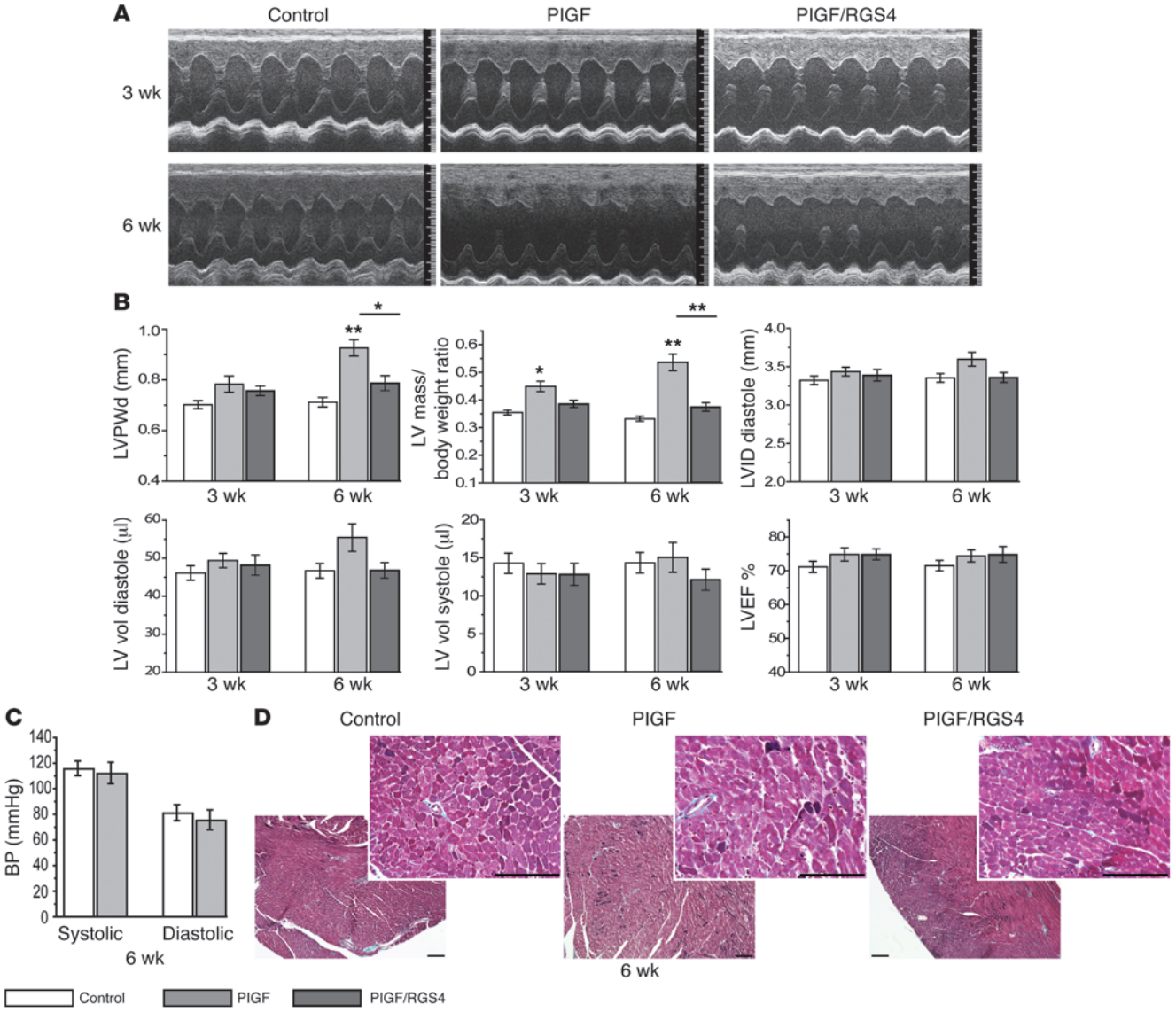

Figure 4

Echocardiographic analysis and assessments of blood pressure and fibrosis in PIGF and PIGF/RGS4 mice. (**A**) M-mode echocardiograms of PIGF, PIGF/RGS4, and control mice at 3 and 6 weeks. (**B**) Echo-determined analysis of LV posterior wall thickness in diastole (LVPWd), LV mass/ body weight ratio, LV diameter (LVID) and LV volume (LV vol) in diastole and/or systole, and LV ejection fraction (EF) in PIGF and PIGF/RGS4 mice at 3 and 6 weeks. n = 16 (PIGF/RGS4 6 wk); 18 (PIGF 6 wk); 28 (PIGF 3 wk); 30 (PIGF/RGS4 3 wk); 44 (control 6 wk); 56 (control 3 wk). (**C**) Systolic and diastolic blood pressure assessments in PIGF mice at 6 weeks of induction compared with control mice. No significant differences in blood pressure were observed between groups. n = 5 per group. (**D**) Representative Masson trichrome staining of LV myocardium after 6 weeks of transgene induction. Note the lack of discernible interstitial fibrosis in PIGF and PIGF/RGS4 mice. Scale bars: 100 μm. $^{*}P < 0.05$, $^{**}P < 0.01$ vs. control or as indicated by brackets.

phosphorylated and sequestered in the cytoplasm in the inactive form, but, once dephosphorylated by calcineurin, they are activated and translocated to the nucleus. NFAT3 is a known downstream effector of calcineurin, when activated by Gαq in response to hypertrophic agonists of GPCR, including Ang II (30, 31). To determine whether calcineurin/NFAT3 activation was induced in PlGF mice, we assessed NFAT3$^{Ser168/170}$ phosphorylation, as previously described (31). Our results showed no decrease in NFAT3 phosphorylation in PlGF mice at 3 or 6 weeks compared with controls (Figure 6, A and C), indicative of no NFAT3 activation in this model. These in vivo results were in agreement with in vitro experiments showing that NO donor treatment did not induce NFAT promoter activity in cultured cardiomyocytes (Supplemental Figure 5). Moreover, these results were further supported by the lack of induction of the fetal program of gene expression: our data showed no evidence of downregulation of α*MHC* or upregulation of *ANP* or β*MHC* transcripts after 3 or 6 weeks of angiogenic stimulation in PlGF mice (Figure 6D). Induction of the fetal program of gene expression is known to accompany hypertrophic Gαq/Ang II signaling due to calcineurin/NFAT activation. Together,

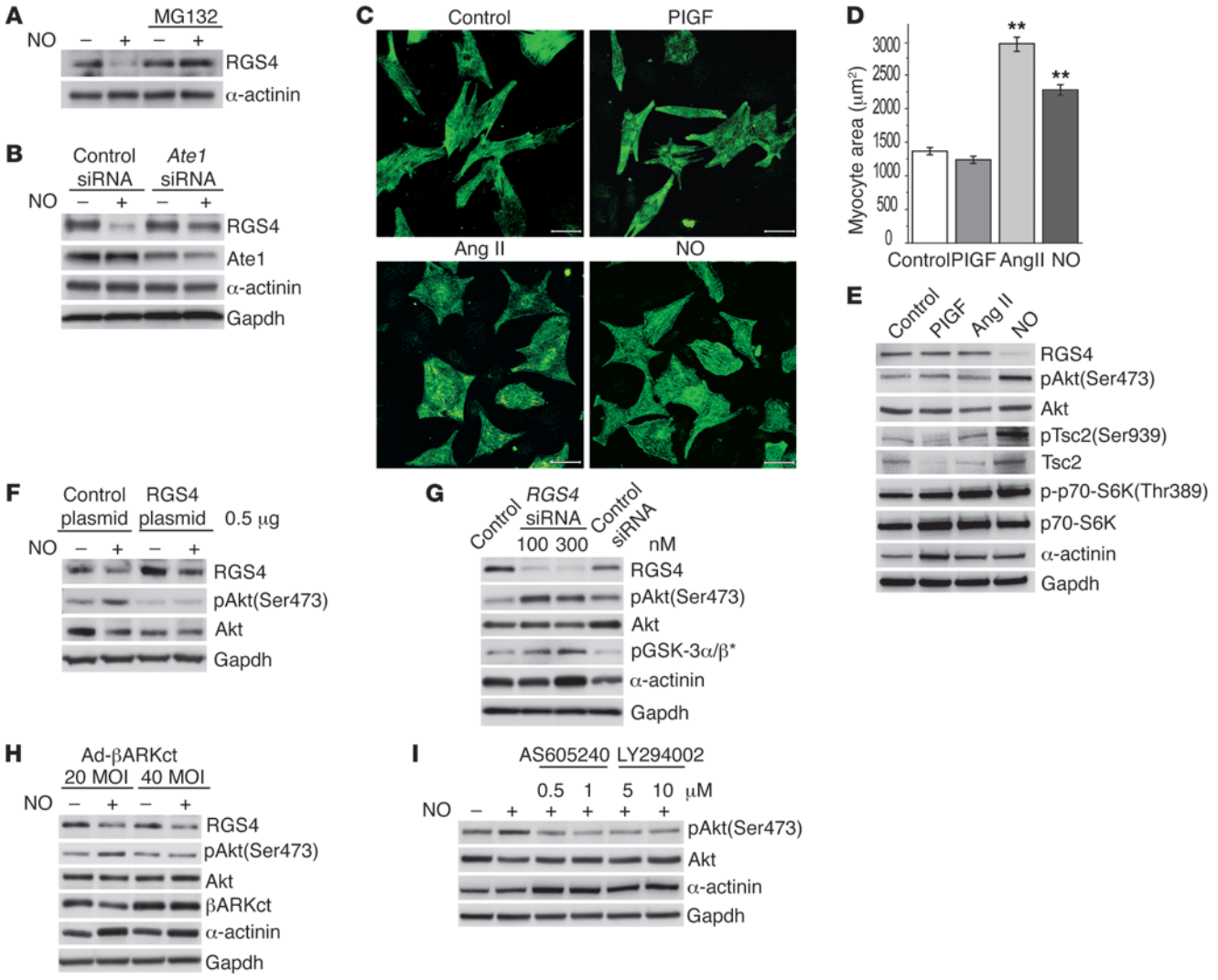

Figure 5

NO mediates cardiomyocyte hypertrophy in culture. (**A**) The proteasomal inhibitor MG132 (20 μM) or (**B**) depletion of *Ate1* with siRNA (200 nM) prevented RGS4 degradation in rat neonatal cardiomyocytes treated for 4 hours with the slow-acting NO donor (NO) DETA-NONOate (100 μM). (**C**) Representative micrographs of rat neonatal cardiomyocytes left untreated or treated with NO donor (100 μM), Ang II (0.5 μM), or PlGF (50 ng/ml) for 24 hours, then immunostained with anti–α-actinin sarcomeric Ab. Scale bars: 50 μm. (**D**) NO donor treatment induced a significant increase in cell surface area compared with untreated or PlGF-treated cells (n = 80 per group). $^{**}P < 0.01$ vs. control and PlGF. (**E**) Akt/mTORC1 pathway activation in NO-treated cardiomyocytes. Representative Western blot analysis for Akt^{Ser473}, $Tsc2^{Ser939}$, and $p70\text{-}S6K^{Thr389}$ phosphorylation after 24 hours of treatment. (**F**) NO donor reduced RGS4 protein level in RGS4-overexpressing cardiomyocytes to control levels, but did not activate Akt. Cardiomyocytes were transfected with 0.5 μg RGS4 plasmid or control plasmid and treated with NO donor for 24 hours. (**G**) Increased Akt^{Ser473} phosphorylation and Akt kinase activity in cardiomyocytes with *RGS4* depleted by siRNA. Akt kinase activity in cell lysates was determined in an in vitro assay using GSK-3 as substrate and Western blotting for GSK-3α/$\beta^{Ser21/9}$ phosphorylation. Asterisk denotes assessment by in vitro kinase assay. (**H**) The Gβγ subunit scavenger βARKct prevented Akt activation in NO-treated cardiomyocytes at higher MOI of Ad-βARKct (40 vs. 20 MOI). (**I**) The PI3Kγ-specific inhibitor AS605240 and the pan-PI3K inhibitor LY294002 prevented Akt^{Ser473} phosphorylation in NO-treated cardiomyocytes.

our data support the conclusion that NO-induced cardiac growth occurs in the absence of Gαq signaling activation, despite the reduction in RGS4 expression.

We next determined whether suppression of angiogenesis inhibits the hypertrophic response in PlGF mice. To address this, transgene expression in PlGF mice for 6 weeks was turned off by reintroducing doxycycline in the diet. At 3 weeks after discontinuation of PlGF stimulation, NO production returned to control levels, and RGS4 degradation and activation of Akt/mTORC1 signaling was prevented (Figure 7, A and B). Taken together, these results indicate that the RGS4/Akt pathway couples cardiac vessel growth with a hypertrophic response in cardiomyocytes.

NOS inhibition with L-NAME or eNOS gene deletion prevents the hypertrophic response, whereas nNOS inhibition with SMTC has no effect on hypertrophic response. To gain further insights into the nature of the hypertrophic mechanism, we tested whether inhibition of NO production impairs the angiogenesis-induced hypertrophic response. Our data pointed to eNOS-derived NO as a source of NO-mediating RGS4

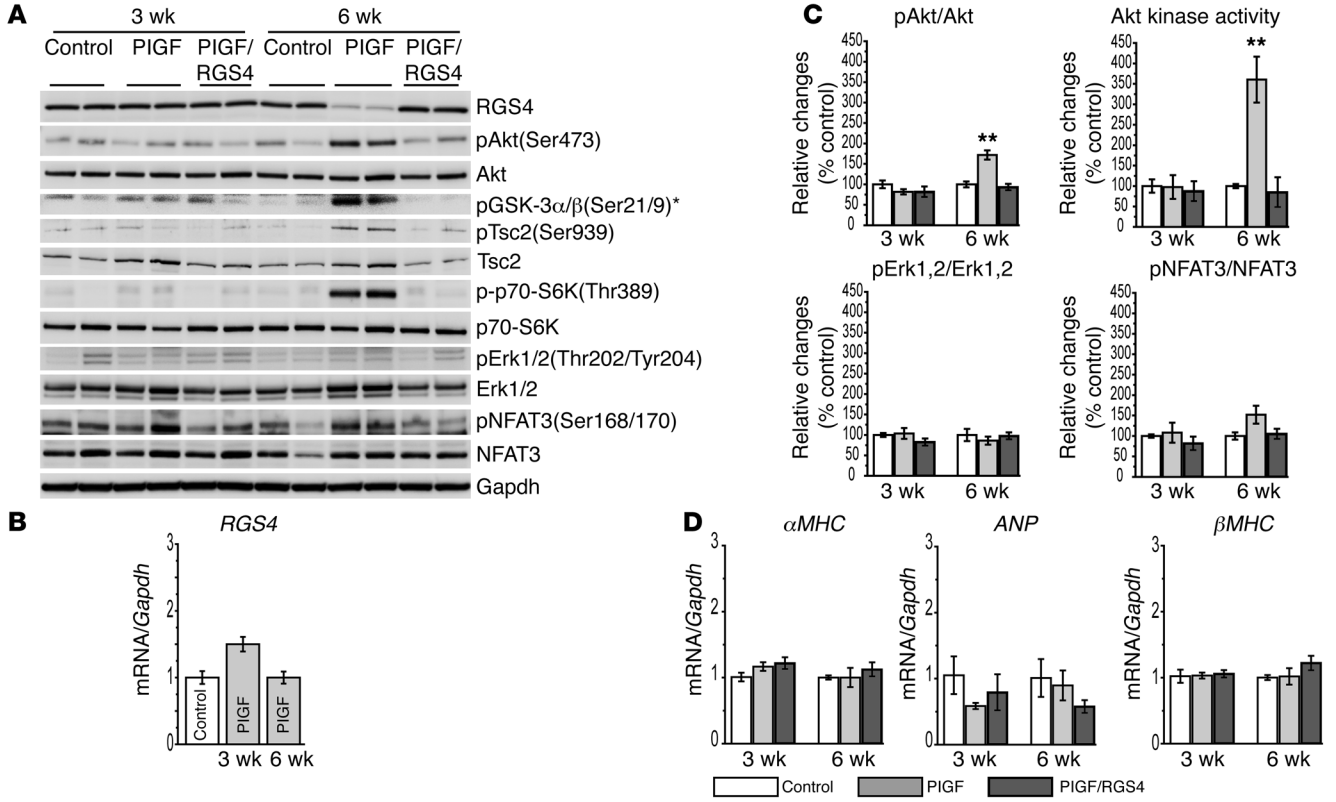

Figure 6

Molecular signature of myocardial hypertrophy subsequent to angiogenic stimulation. (**A**) Representative Western blot analysis of RGS4, Akt^{Ser473}, GSK-3α/β$^{Ser21/9}$, Tsc2^{Ser939}, p70-S6K^{Thr389}, Erk1/2$^{Thr202/Tyr204}$, and NFAT3$^{Ser168/170}$ expression in PlGF, PlGF/RGS4, and control hearts at 3 and 6 weeks. At 6 weeks, RGS4 level was reduced and Akt/mTORC1 pathway was activated in PlGF mice, whereas RGS4 level was restored and Akt activation was blunted in PlGF/RGS4 mice. Asterisk denotes assessment by in vitro kinase assay. (**B**) *RGS4* mRNA expression in PlGF mice at 3 and 6 weeks. (**C**) Quantification of relative changes in Akt, Erk, and NFAT activation in PlGF, PlGF/RGS4, and control mice at 3 and 6 weeks, as determined by Western blotting. Akt kinase activity was determined by quantification of GSK-3α/β$^{Ser21/9}$ phosphorylation (in vitro assay) relative to total Akt. n = 4–10 per group. (**D**) Relative mRNA expression of α*MHC*, *ANP*, and β*MHC* in PlGF and PlGF/RGS4 mice after 3 and 6 weeks induction compared with control mice. n = 6 per group. $^{**}P < 0.01$ vs. control.

degradation (Figure 2); however, it has been previously suggested that nNOS-derived NO may regulate RGS4 level (8). Therefore, to clarify the role of eNOS in the angiogenesis-driven hypertrophic response, we chose a pharmacological approach using the nonselective NOS inhibitor L-NAME and a highly selective nNOS inhibitor, S-methyl-L-thiocitrulline (SMTC; ref. 32), in parallel with an *eNOS* gene knockout mouse model. Treatment with L-NAME or SMTC was carried out in PlGF mice subsequent to angiogenesis and prior to hypertrophic stimulation, corresponding to the last 3 weeks of the 6-week induction period. Conditional PlGF expression in *eNOS*$^{-/-}$ mice (referred to herein as PlGF-*eNOS*$^{-/-}$ mice) was induced at 5 weeks of age for 6 weeks by doxycycline withdrawal.

Although there was a modest decrease in the angiogenic response in L-NAME–treated PlGF mice and PlGF-*eNOS*$^{-/-}$ mice compared with untreated PlGF mice, the increase in the capillary/myocyte ratio was significantly higher compared with L-NAME–treated or *eNOS*$^{-/-}$ controls (Figure 8A). In SMTC-treated PlGF mice, angiogenesis was not affected (Figure 8A). Interestingly, while L-NAME treatment or *eNOS* gene deletion significantly prevented NO release, as measured by PKG activity, SMTC treatment had no effect (Figure 8B). Additionally, we found that L-NAME significantly reduced PKG activity in PlGF/RGS4 mice (Supplemental Figure 6).

We next assessed the effect of L-NAME, *eNOS* gene deletion, and SMTC on myocardial hypertrophy. In L-NAME–treated PlGF mice, we observed a direct relationship between reduced NO production and restoration of RGS4 to normal levels (Figure 8C). In PlGF-*eNOS*$^{-/-}$ mice, RGS4 protein remained unchanged compared with *eNOS*$^{-/-}$ control mice. Interestingly, in SMTC-treated PlGF mice, the RGS4 level was significantly reduced (Figure 8C), in agreement with increased NO production in these mice. Consistent with the RGS4 protein levels observed, Akt^{Ser473} phosphorylation returned to control levels in L-NAME–treated PlGF mice, was unchanged in PlGF-*eNOS*$^{-/-}$ mice, and was significantly increased (approximately 1.7-fold) in SMTC-treated PlGF mice (Supplemental Figure 7). Similarly, determination of Akt kinase activity in LV tissue lysates, a more sensitive approach, showed normalization of Akt activity in L-NAME–treated PlGF and PlGF-*eNOS*$^{-/-}$ mice, whereas in untreated or SMTC-treated PlGF mice, Akt activation increased approximately 3.5-fold (Figure 8D). In accord with reduced Akt activity in L-NAME–treated PlGF mice or PlGF-*eNOS*$^{-/-}$ mice, activation of the mTORC1 target p70-S6K, as measured by p70-S6K^{Thr389} phosphorylation, was completely abolished (Figure 8C).

Consistent with the blunted activation of Akt/mTORC1 signaling, L-NAME treatment significantly decreased the increase in LV

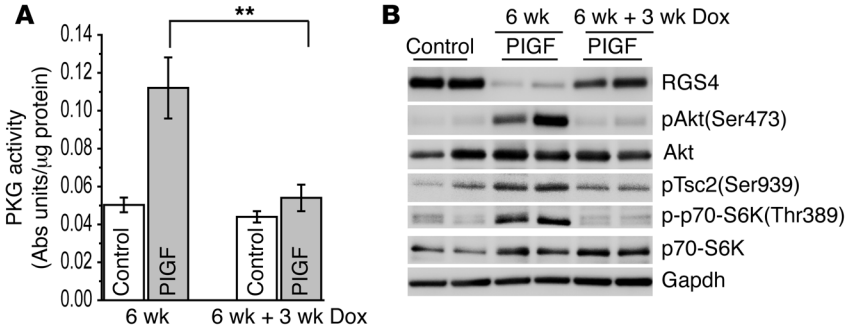

Figure 7
Suppression of angiogenic stimulation prevents the hypertrophic response. (**A**) PKG activity in LV tissue lysates in PlGF mice after 6 weeks induction and 6 weeks induction followed by 3 weeks suppression with doxycycline (Dox). n = 8–14 per group. $^{**}P < 0.01$. (**B**) Restored RGS4 level and inhibition of Akt/mTORC1 activation after suppression of angiogenic stimulation with Dox for 3 weeks in PlGF mice after 6 weeks induction. Shown are Western blot analysis of RGS4, Akt^{Ser473}, $Tsc2^{Ser939}$, and $p70\text{-}S6K^{Thr389}$.

wall thickness and mass, whereas *eNOS* gene deletion completely inhibited it (Figure 8, E and F). SMTC treatment in PlGF mice did not prevent cardiac enlargement in response to myocardial angiogenesis and increased NO production (Figure 8, E and F). It has previously been reported that $eNOS^{-/-}$ mice progressively develop myocardial hypertrophy as they age (33); however, this did not interfere with our data (Figure 8, E and F, compare $eNOS^{-/-}$ control and untreated control), due to the fact that our experiments were done in younger mice (at 10–11 weeks of age, as opposed to 27–30 weeks, when myocardial hypertrophy is apparent). Similarly, we did not observe cardiac hypertrophy in L-NAME– or SMTC-treated control groups versus the untreated control (Figure 8, E and F). Moreover, no significant differences in heart rates were found between groups (Supplemental Table 1). Together, our data suggest that eNOS is the source of NO release in our model and that nNOS is not involved.

Discussion

Collectively, our present data revealed novel endothelial-derived, NO-dependent hypertrophic signaling to cardiomyocytes. By inducing NO-mediated degradation of RGS4 and consequent activation of Gβγ/PI3Kγ/Akt/mTORC1 signaling, increased vascularity promotes myocardial growth in the absence of traditional hypertrophic stimuli (Figure 9).

The conditional mouse models used in this study allowed us to determine a temporal relationship between angiogenesis and the hypertrophy onset in the adult heart. The observation that the increase in vasculature preceded the onset of hypertrophy was in agreement with our previous PR39 model (2) and an earlier report that used thyroxin treatment to induce the angiogenic response in the heart (34). The hypertrophied myocardium in this study revealed a remarkable growth of the coronary arterial tree through distal branching, increased capillary density, and significant cardiomyocyte hypertrophy. The hearts demonstrated preserved LV contractile function, no discernible fibrosis, and no induction of markers associated with pathological hypertrophy (i.e., *ANP* and β*MHC*). They also had a slightly decreased ratio of LV radius to wall thickness (1.97 ± 0.07 vs. 2.42 ± 0.07 in controls; $P < 0.001$), similar to the physiological hypertrophy developed during strength-based exercise (e.g., wrestling and weight lifting) or with the early adaptive hypertrophic response to hypertension (35–37). However, our results do not exclude the possibility of a later decline in cardiac function, with longer stimulation due to an imbalance of the growth response (38) and/or negative inotropic properties of NO that have previously been reported (2).

Our observation that direct treatment of cardiomyocytes with PlGF did not result in hypertrophic response is in agreement with previous reports and might be explained by the lack of VEGFR1 expression on cardiomyocytes (24, 25). Moreover, it has been suggested that PlGF primarily stimulates endothelial cells and fibroblasts that in turn support cardiomyocyte hypertrophy through a paracrine-mediated mechanism (24, 25). In pressure overload, one such paracrine growth factor might be interleukin-6 released by fibroblasts (25).

Accornero et al. previously reported that cardiomyocyte PlGF overexpression in the absence of pressure overload did not promote angiogenesis or cardiac hypertrophy (25); the discrepancy between their results and ours may be a consequence of differences in the control of transgene expression, variability between mouse strains, or a combination of both. In our study, the conditional Tet-OFF expression of *PlGF* transgene was controlled by a traditional CMV minimal promoter coupled to *TRE*, whereas Accornero et al. used a modified *MHC* promoter linked to *TRE* in order to induce low levels of transgene expression (25). It is possible that, in the absence of pressure overload, attenuated *PlGF* transgene expression does not promote or sustain myocardial angiogenesis. Moreover, differences in the genetic background between mouse strains (C57BL/6 in the present study versus the more cardioprotective strain FVB/N used by Accornero et al.; ref. 25) might be a source of variability in angiogenic response (39). Regardless, the notion of cardiac hypertrophy subsequent to angiogenic stimulation is supported by our previous study (2), results using thyroxin treatment (34), and a recent report by Bry et al. of transgenic VEGFB overexpression in the rat myocardium (40).

Although RGS4 loss- and gain-of-function conditional mouse models both showed increased angiogenesis/arteriogenesis and NO release, loss of RGS4 in the PlGF mice activated hypertrophic signaling, whereas RGS4 gain of function by stabilizing RGS4 level prevented Akt/mTORC1 activation and myocardial hypertrophy in the PlGF/RGS4 mice. Hypertrophy induction was partially inhibited by the NOS inhibitor L-NAME and was abolished in $eNOS^{-/-}$ mice, although angiogenesis was still induced. Although eNOS is constitutively expressed both in the vascular endothelium and in cardiomyocytes (41, 42), we showed that eNOS was mostly expressed in the endothelium, and its expression was upregulated by angiogenic stimulation, whereas cardiomyocytes showed no increase in eNOS expression. Moreover, the likelihood that VEGFR1 is not expressed on cardiomyocytes but is required for PlGF-induced eNOS activation (43) further indicates that NO release is primarily endothelium dependent. Consistent with this notion was our observation that PlGF treatment in cell culture did not reduce RGS4 level.

A previous study by Hu et al. suggested that nNOS-derived NO might be involved in RGS4 degradation (8). This observation was based on cell culture experiments done in 3T3 cells overexpressing

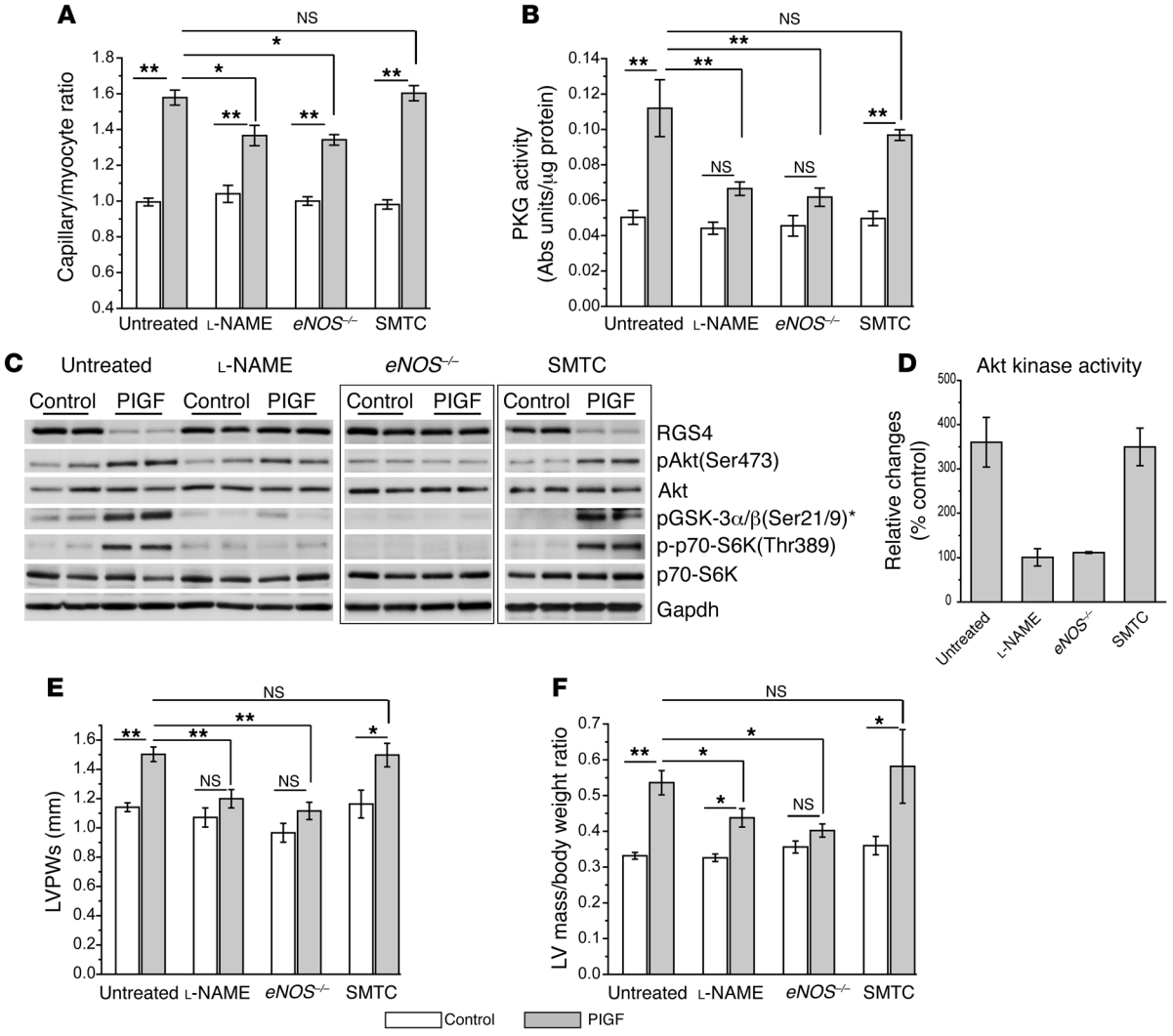

Figure 8

Cardiac hypertrophy reduction by L-NAME treatment or *eNOS* gene deletion. L-NAME (0.5 g/l drinking water) or SMTC (10 mg/kg/d drinking water) was given during the last 3 weeks of the 6-week induction period. (**A**) Capillary/myocyte ratio at 6 weeks for untreated PIGF, L-NAME–treated PIGF, PIGF-*eNOS*$^{-/-}$, and SMTC-treated PIGF mice and their appropriate controls. (**B**) PKG activity in LV tissue lysates at 6 weeks. L-NAME–treated PIGF and PIGF-*eNOS*$^{-/-}$ mice showed a significant decline in NO production. n = 5–14 per group. (**C**) Comparative Western blot analysis of RGS4, Akt^{Ser473}, GSK-3α/β$^{Ser21/9}$, and p70-S6K^{Thr389} expression at 6 weeks. Asterisk denotes assessment by in vitro kinase assay. (**D**) Akt kinase activity, determined by quantification of GSK-3α/β$^{Ser21/9}$ phosphorylation relative to total Akt in Western blots. Data represent percent of respective control for each group. (**E**) Echo-determined LV posterior wall thickness in systole (LVPWs) and (**F**) LV mass/body weight ratio. n = 4 (SMTC control); 5 (PIGF-*eNOS*$^{-/-}$); 7 (SMTC PIGF); 8 (L-NAME PIGF and *eNOS*$^{-/-}$ control); 10 (L-NAME control); 18 (untreated PIGF); 44 (untreated control). *P < 0.05, **P < 0.01.

RGS4 under Tet-OFF control. The 3T3 cells apparently express only nNOS, and decreasing intracellular NO production using either the NOS inhibitor N^G-monometyl-L-arginine (LMMA) or the highly selective nNOS inhibitor N3411 significantly increased RGS4 levels. Moreover, there was an apparent increase in RGS4 levels in lungs from *nNOS*$^{-/-}$ versus wild-type mice, despite the presence of eNOS and iNOS in these mice (8). However, these results do not completely rule out the contribution of other NOS isoforms or a potential extracellular source of NO in a more complex intercellular paracrine signaling scheme. Here, we demonstrated that eNOS-released NO controlled RGS4 degradation in cardiomyocytes and that nNOS was not involved. Although we did not investigate in detail how endothelium-derived NO targets RGS4 degradation within cardiomyocytes, we speculate that the NO-RGS4 interaction is facilitated by localization of RGS4 at the plasma membrane. This is supported by spatial modeling of G protein activation (44) and the RGS4-mediated "kinetic scaffolding" mechanism (45). Furthermore, in a manner similar to that previously described for RGS2 (46), RGS4 translocation from the cytoplasmic to the plasma membrane may actually be induced by activated PKG and could represent a potential mechanism underlying regulation of RGS4 degradation by NO. However, further studies will be needed to clarify this.

Although previous studies have shown that RGS4 overexpression inhibits Gαq signaling in response to GPCR agonists (47, 48),

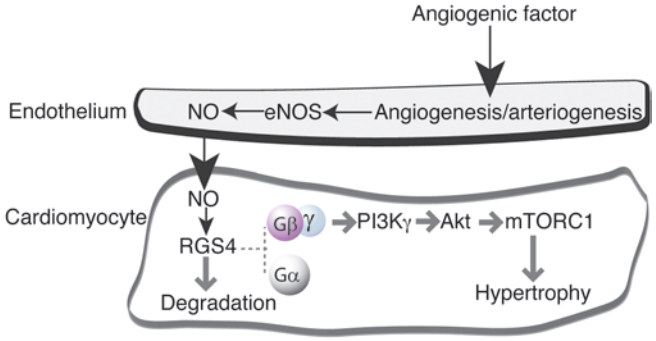

Figure 9
Endothelium-to-cardiomyocyte communication paradigm. Increased RGS4 degradation induced by NO release subsequent to angiogenesis/arteriogenesis in the heart acts as a hypertrophic switch that promotes a growth response in cardiomyocytes. Loss of RGS4 relieves G protein inhibition; thus, Gα/Gβγ subunits are prone to propagate hypertrophic signaling. This is most likely initiated by freely dissociated Gβγ subunits through activation of the PI3Kγ/Akt/mTORC1 pathway. This mechanism occurs in the absence of traditional hypertrophic stimuli.

pressure overload (49), and Gαq transgenic overexpression (50), reciprocal reduction in RGS4 does not appear to increase Gq signaling, based on our present findings. However, it is important to recognize that excess gain of function and more physiologic loss of function do not necessarily have opposite effects. The NO-regulated RGS4 loss-of-function mechanism that induced hypertrophy in our model is distinct from both GPCR agonist– and Gαq overexpression–induced hypertrophy. Our model lacks LV pressure overload and GPCR-coupled GTP loading that leads to Gαq activation.

Although the reduction in RGS4 could potentially release Gαq, it might not be sufficient to achieve significant hypertrophic potential. This is supported by previous studies showing that only higher-level Gαq overexpression (wild type or constitutively active) resulted in cardiac hypertrophy and increased expression of hypertrophic markers (51, 52). However, our present results do not exclude the possibility that more prolonged angiogenic stimulation might eventually increase Gαq signaling or might augment Gαq signaling under conditions of pressure overload.

More direct evidence of RGS4 protein degradation has been reported in human breast carcinomas, in which RGS4 is used as a marker for breast cancer invasiveness. Loss of RGS4 in cancer cells results in aberrant Gβγ-induced Rac activation that is rescued by proteasomal inhibitor or Gβγ scavenger peptide (53, 54). Although the causes of RGS4 degradation in advanced breast cancer remain unknown, an interesting observation is that increased angiogenesis and NO production occur at about the same time (55). Nevertheless, additional functions of RGS4 beyond simply accelerating GTPase activity are starting to emerge (56).

The results of this study present a new perspective on the existing paradigm of the role of NO in growth regulation, which has focused on its antihypertrophic effects in cardiomyocytes. In cardiomyocytes, the antihypertrophic effect of NO is exerted by sGC/cGMP/PKG activation that appears to act as a brake, reducing hypertrophic stimulation in response to hemodynamic stress (57). PKG inhibits the calcineurin/NFAT pathway involved in the development of pathological hypertrophy (58–61). In this study, we used PKG kinase activity, as a readout of NO release, to demonstrate a direct correlation between NO production and cardiac hypertrophy. However, the observed effect occurred in the absence of any traditional hypertrophic stimuli, and it might not involve pathologic signaling. PKG activity assessed in heart tissue lysates might be confounded by PKG activity in cells other than cardiomyocytes (e.g., smooth muscle cells). Although ANP can also activate cGMP-dependent PKG activity, the absence of ANP induction in our study indicates that NO was likely the main source for PKG activation.

Finally, our findings support a novel mechanism mediated by endothelium-released NO that leads to Akt/mTORC1 pathway activation in cardiomyocytes as a coupling mechanism between the extents of cardiac vasculature and myocyte growth. Intriguingly, this most likely occurs through Gβγ-dependent PI3Kγ activation once the increased NO level controls RGS4 degradation through the Arg/N-end rule pathway of protein degradation. Interestingly, we demonstrated a physiological type of myocardial hypertrophy in our model that was consistent with Akt pathway involvement in physiological rather than pathological hypertrophy. From a clinical standpoint, this study is important because it suggests that increased cardiac vasculature and NO release — beyond augmenting blood perfusion — could shift the hypertrophic paradigm from pathological to physiological growth through Akt activation, while potentially inhibiting pathological progression through sGC/cGMP/PKG activation.

Methods

PlGF and PlGF/RGS4 conditional transgenic mice

The Tet-OFF responder mouse lines *TRE-PlGF* and *TRE-PlGF/RGS4* were generated by subcloning murine *PlGF* cDNA (GenBank NM_008827; provided by P. Carmeliet, Katholieke Universiteit Leuven, Leuven, Belgium; ref. 62) and *LacZ* cDNA, and *PlGF* cDNA and human *RGS4* cDNA (GenBank U27768), respectively, into bidirectional pBI Tet Vector (Clontech) sensitive to *tTA*. In cell culture, inducible *TRE-PlGF/LacZ* and *TRE-PlGF/RGS4* vectors were expressed in the Tet-OFF MEF/3T3 cell line (Clontech) in the absence of doxycycline. The *TRE-PlGF/LacZ* and *TRE-PlGF/RGS4* constructs were then microinjected into fertilized mouse eggs (Transgenic Mouse Service, Yale). *tTA/PlGF* and *tTA/PlGF/RGS4* mice were produced by crossing the driver line *αMHC-tTA* (2) with *TRE-PlGF* and *TRE-PlGF/RGS4* mice. Transgenic mouse lines were generated in the C57BL/6 background and maintained by mating hemizygous transgenic mice (Tg/0) with wild-type C57BL/6 mice (0/0). Genotyping was performed by Transnetyx (Cordova) using a quantitative real-time PCR–based (qPCR-based) system to detect the presence or absence of a target sequence within each sample. The following target sequences were used: *LacZ* (*TRE-PlGF* line), human *RGS4* cDNA exon-exon junction (*TRE-PlGF/RGS4* line), and *tTA* (*αMHC-tTA* line). The Tet-OFF conditional inducible cardiac PlGF model in the *eNOS* knockout strain (PlGF-*eNOS*$^{-/-}$ mice) was created by mating hemizygous responder *TRE-PlGF* mice and driver *αMHC-tTA* mice with homozygous *eNOS*$^{-/-}$ mice (C57BL/6 background, The Jackson Laboratory). After backcrossing with *eNOS*$^{-/-}$ mice to restore homozygosity, double-transgenic mice were generated by crossing *TRE-PlGF*$^{+}$*eNOS*$^{-/-}$ mice with *αMHC-tTA*$^{+}$*eNOS*$^{-/-}$ mice. Transgene expression of *PlGF/LacZ* or *PlGF/RGS4* was repressed during embryonic and postnatal development by doxycycline in diet (200 mg/kg; Bio-Serv) and induced by normal chow diet feeding beginning at 5 weeks of age. *PlGF* transgene expression was determined by RT-PCR using the following primers: forward, 5′-GATGCTGGTCATGAAGCTGTTC-3′; reverse, 5′-TCGTCTCCAGAATAGGTCTGCA-3′. PlGF protein was determined by Western blot. *RGS4* transgene expression was determined by qPCR using the following primers: forward, 5′-CCAGAGA-

GTGAGCCAAGAGG-3′; reverse, 5′-ATCTTTTTGGCCTTGGGACT-3′. *RGS4* endogenous gene expression was determined by qPCR using the following primers: forward, 5′-ACACAGAGGCAGGGAGCCCAA-3′; reverse, 5′-GCGGCAGGCAGCATGGACAC-3′. RGS4 protein was determined by Western blotting. Mice were treated with L-NAME (0.5 g/l; Sigma-Aldrich) or with SMTC (10 mg/kg/d; Sigma-Aldrich) in the drinking water (63–65). Littermates inheriting only responder or driver transgene were used as controls and were treated similarly.

Histological assessments

Capillary density. Capillary density was determined on serial 5-μm heart sections (fixed in 4% paraformaldehyde and embedded in paraffin) stained with isolectin B4 (IB4; Sigma-Aldrich) and anti-laminin Ab (Sigma-Aldrich) and reported as capillary/myocyte ratio. Suitable transversal cross-sections for counting contained nearly circular myocytes and clear round-shaped capillaries. Quantification was done on ×40 fields divided into 12 squares (2,600 μm^2 each), using 4–5 fields per mouse and 3–4 mice per group.

Cardiomyocyte size. Cardiomyocyte size was determined by cross-sectional area measurements on heart sections immunostained with anti-laminin antibody or after myocyte isolation by enzymatic dissociation using the Langendorff apparatus (66). After isolation, myocytes were plated on laminin-coated plates, fixed (4% paraformaldehyde), and stained with anti–α-actinin sarcomeric Ab and DAPI. Cell surface area was measured in captured images with Nikon Eclipse 80i microscope and analyzed with NIS-Elements software.

Fibrosis. Fibrosis was determined by Masson trichrome staining on paraffin-embedded sections.

Inflammation. Inflammation was detected on frozen sections (embedded in OCT compound) by double immunostaining with specific antibodies against CD45 (eBioscience) for leukocytes and CD31 (Millipore) for endothelium.

eNOS expression. Expression of eNOS was determined on serial 5-μm heart sections (fixed in 4% paraformaldehyde and embedded in paraffin) stained with IB4 (Sigma-Aldrich) and anti-eNOS Ab (BD Transduction Laboratories). Quantification of eNOS expression in the endothelium was determined in captured images with Zeiss confocal microscope, analyzed using Image J software, and reported as ratio of eNOS to IB4 staining.

Echocardiography

Mice were sedated with 1% isoflurane in oxygen. Echo images were acquired in M-mode following standard procedures with the VisualSonics Vevo 770 high-resolution in vivo microimaging system.

Blood pressure measurements

A 1.4-F Mikro-tip pressure-volume catheter (Millar Instrument) was introduced into the proximal portion of the ascending aorta via the right common carotid artery to determine systolic and diastolic blood pressure. Mice were anesthetized with 1.5% isoflurane, and body temperature was maintained at 36.5°C by standard methods. Data were recorded with LabChart 6.0 software.

High-resolution X-ray CT (micro-CT)

Mice were heparinized by intraperitoneal injection (50 μl heparin per mouse; 1,000 U/ml) and anesthetized by isoflurane inhalation. Postmortem intracoronary perfusion was performed on isolated heart connected to a simplified Langendorff perfusion system. Briefly, a polyethylene tube (PE50) was inserted into the LV via the mitral valve to remove the LV load. The heart was arrested at the end of the diastole via brief perfusion of KCl (100 mM; ref. 67) and was immediately flushed by switching the perfusion solution to 1 ml heated saline (37°C), followed by 100 μl adenosine (3 mg/ml) and 1 ml 4% paraformaldehyde. The perfusion was then changed to 50 μl, 20% bismuth (37°C in 5% gelatin; ref. 68), and the pressure was set at 100–110 mmHg for 5 seconds. The whole heart was quickly immersed in a cold saline circulation bath (0°C) for 3 minutes, so that the contrast medium solidified under the perfusion pressure. The time required to complete these procedures was less than 15 minutes. Finally, the heart was removed and immersed in 2% paraformaldehyde overnight at 4°C.

Micro-CT scanning. Individual hearts were staged in a high-resolution micro-CT scanner (GE eXplore Locus SP; GE Healthcare) with a cone beam filtered back projection algorithm, set to an 8-μm effective detector pixel size. Micro-CT was performed with 60-kVp X-ray tube voltage, 100-μA tube current, 2,960 milliseconds per frame, 1 × 1 detector binning model, 360° angle, and 0.5° increments per view.

Image processing. Microview Software (GE Healthcare) was used to reconstruct raw data with 16 × 16 × 16 μm^3 voxel, and images were calibrated by standard radioattenuation values (air, water, and bone). The initial reconstructed micro-CT data were transferred to Advanced Workstation (AW4.4; GE Healthcare) for segmentation. The segmented coronary artery was rebatched into axial slices. Detailed morphometric data on the diameter, area, number of vessels, and distribution of different-sized vessels were extracted using modified ImageJ software. The distribution of the relative arterial vessel number was automatically calculated with a built-in algorithm. Data were expressed as the number of vascular segments, representing the total number of vessels of a specified diameter counted in the whole heart.

Vascular morphometric quantifications. The 3D vascular tree was reconstructed using a recently published vascular tree reconstruction algorithm (69). The overall process consisted of 2 parts: (a) vessel detection and skeletonization and (b) connectivity. For vessel detection, we merged the classic method described by Frangi et al. (70) with the skeletonization method described by Lee at al. (71). For vessel connectivity, we used our recently developed and validated physiologically constrained method that was described in detail previously (69). This method takes as inputs a set of disconnected vessel fragments (the output of the detection/skeletonization algorithms) and connects them to form an optimal 3D vascular tree by selecting the candidate vascular tree that minimizes the overall energy required to perfuse the heart muscle — a constraint that is formally derived from Murray's hypothesis (72). This method was previously shown to have statistically significant performance improvements over prior simpler methods (e.g., minimum spanning tree) in this type of image (69). From the resulting 3D-connected model of the vascular tree, we proceeded to compute detailed morphometric descriptors of the vascular anatomy. In particular, we defined a vessel segment to be the vessel that connects 2 subsequent bifurcation points. Next, we characterized the vessel segments by computing their diameter, length, and branching level (the former 2 concepts are self-explanatory). We defined branching level as a number, starting at 1 (at the arterial root level) and increasing by 1 at each subsequent vessel bifurcation. Hence, a larger vessel (e.g., the left anterior descending artery) has a branching level of 2 (1 bifurcation down from the root of the tree), whereas in general, smaller vessels have higher branching levels. Figure 1D shows a sample reconstruction of the vascular tree, in which vessel segment color is indicative of its branching level. The standard rainbow colormap ranges from blue (level 1) to red (level 80), with appropriate interpolation in between, following the same pattern as the rainbow.

Hypertrophic marker gene expression

Analysis of hypertrophic marker gene expression was performed by qPCR. Total RNA was isolated from LV samples with QIAzol/RNeasy mini kit (Qiagen) and reversed transcribed (500 ng of total RNA) using iScript cDNA synthesis kit (Bio-Rad Laboratories). qPCR was carried out using iQ SYBR Green supermix kit (Bio-Rad Laboratories) in a CFX96 real-time PCR detection system (Bio-Rad Laboratories). The following primers were used: *GAPDH* forward, 5′-AACTTTGGCATTGTGGAAGG-3′; *GAPDH* reverse,

5′-ACACATTGGGGGTAGGAACA-3′; *ANP* forward, 5′-CCTAAGCCCTTGTGGTGTGT-3′; *ANP* reverse, 5′-CAGAGTGGGAGAGGCAAGAC-3′; β*MHC* forward, 5′-TGCAGCAGTTCTTCAACCAC-3′; β*MHC* reverse, 5′-TCGAGGCTTCTGGAAGTTGT-3′; α*MHC* forward, 5′-GAGGACCAGGCCAATGAGTA-3′; α*MHC* reverse, 5′-GCTGGGTGTAGGAGAGCTTG-3′.

Cardiomyocyte culture experiments

Cell culture reagents. The NO donor DETA-NONOate was from Cayman Chemical Co.; MG132 was from Calbiochem; *Ate1* siRNA, *RGS4* siRNA, and AllStars Negative Control siRNA were from Qiagen; recombinant mouse PlGF-2 was from R&D Systems; AS605240, LY294002, and Ang II were from Sigma-Aldrich; Ad-βARKct was provided by W. Koch (Thomas Jefferson University, Philadelphia, Pennsylvania, USA; ref. 27); reporter vectors pNFAT-SEAP, pTAL, and pSEAP were from Clontech; RGS4 plasmid was from UMR cDNA Resource Center; and control pcDNA3.1$^+$ plasmid was from Invitrogen.

Neonatal rat cardiomyocytes. Neonatal rat cardiomyocytes were isolated from 2-day-old Sprague-Dawley rats using the Neonatal Cardiomyocyte Isolation System (Worthington Biochemical Corp.; ref. 2). Isolated cardiomyocytes were plated on fibronectin-coated plates and cultured for 24 hours in DMEM supplemented with 10% FBS. Experiments were done 24–48 hours after isolation. Cardiomyocytes were treated with NO donor, Ang II, or PLGF in serum-free medium for 24 hours or as indicated otherwise.

Transfection of siRNA. Transfection of siRNA was carried out using TransPass R2 reagent (New England Biolabs).

Transfection of RGS4 plasmid. Transfection of RGS4 plasmid was carried out using nucleofector kit (Lonza).

Transcriptional activity of NFAT. Transcriptional activity of NFAT was determined using the pathway profiling system with secreted alkaline phospahatase SEAP reporter (Clontech).

Cell size measurements in culture. Cardiomyocytes treated as indicated were fixed in 4% PFA and permeabilized with 2% PFA, 0.1% Triton X-100, and 0.1% NP-40. Morphological and morphometric analysis were carried out by immunostaining with anti–α-actinin sarcomeric Ab (1:50; Sigma-Aldrich) and visualization with Zeiss confocal microscope. The myocyte surface area was measured in captured images using Image J software.

Western blotting

Immunoblotting. Proteins, isolated cardiomyocytes, or LV tissue homogenates were extracted in RIPA lysis buffer supplemented with protease inhibitor cocktail (Roche). The lysates were clarified by ultracentrifugation (20,000 *g*, 15 minutes at 4°C), and 30 μg protein extract, determined by BCA assay, was subjected to SDS-PAGE. After transfer to Immobilon membranes (Millipore), the membranes were blocked with 5% nonfat dried milk in TBS (pH 7.4) containing 0.1% Tween 20, and immunoblotted using specific antibodies against RGS4 (from Millipore and Abcam; also provided by S. Mumby, UT Southwestern Medical Center, Dallas, Texas, USA); PlGF-2 (R&D Systems); Akt (Millipore); Akt^{Ser473} (Epitomics); Tsc2, Tsc2^{Ser939}, p70-S6K, and p70-S6K^{Thr389} (Cell Signaling); Gapdh (Research Diagnostics); GRK2, Ate1, NFAT3, and NFAT3$^{Ser168/170}$ (Santa Cruz Biotechnology); α-actinin sarcomeric (Sigma-Aldrich); and eNOS, nNOS, and iNOS (BD Transduction Laboratories). Immunoreactive bands were visualized using horseradish peroxidase–conjugated secondary antibody and enhanced chemiluminescent substrate (Pierce). Images were captured with G:Box gel imaging system and analyzed with GeneTools software (Syngene).

Akt kinase activity. Akt kinase activity was assessed by immunoprecipitation with anti-Akt^{Ser473} antibody, followed by an in vitro kinase assay using GSK-3 as substrate (Cell Signaling).

PKG kinase activity. PKG kinase activity was determined in ELISA format with a peroxidase-coupled anti–phospho–G kinase substrate$^{Thr68/119}$ monoclonal antibody as reporter (Cyclex Co. Ltd.).

Statistics

Data are presented as mean ± SEM. Differences among multiple groups were assessed using 1- or 2-way ANOVA followed by Bonferroni post-hoc test for multiple comparisons. Comparisons between 2 independent groups were performed using a 2-sample *t* test. All *P* values were calculated using 2-tailed statistical tests. Differences were considered significant for *P* values less than 0.05. Data were analyzed using IBM SPSS Statistics 19.00.

Study approval

All animal experiments were performed under a protocol approved by the Institutional Animal Care and Use Committee of Yale University.

Acknowledgments

We thank Monica Palmeri for technical assistance. We are grateful to Peter Carmeliet for PlGF cDNA plasmid, Susanne Mumby for antibody against RGS4, Walter Koch for Ad-βARKct, and David Kass for helpful discussions. This work was supported by a start-up fund Section of Cardiovascular Medicine, Yale School of Medicine (to D. Tirziu).

Received for publication May 31, 2012, and accepted in revised form January 10, 2013.

Address correspondence to: Daniela Tirziu, Yale Cardiovascular Research Center, 300 George Street, New Haven, Connecticut 06510, USA. Phone: 203.737.2627; Fax: 203.737.6236; E-mail: Daniela.Tirziu@yale.edu.

1. Tirziu D, Giordano FJ, Simons M. Cell communications in the heart. *Circulation*. 2010;122(9):928–937.
2. Tirziu D, et al. Myocardial hypertrophy in the absence of external stimuli is induced by angiogenesis in mice. *J Clin Invest*. 2007;117(11):3188–3197.
3. Hao J, et al. Regulation of cardiomyocyte signaling by RGS proteins: differential selectivity towards G proteins and susceptibility to regulation. *J Mol Cell Cardiol*. 2006;41(1):51–61.
4. Mittmann C, et al. Expression of ten RGS proteins in human myocardium: functional characterization of an upregulation of RGS4 in heart failure. *Cardiovasc Res*. 2002;55(4):778–786.
5. Owen VJ, et al. Expression of RGS3, RGS4 and Gi alpha 2 in acutely failing donor hearts and end-stage heart failure. *Eur Heart J*. 2001;22(12):1015–1020.
6. Lee MJ, et al. RGS4 and RGS5 are in vivo substrates of the N-end rule pathway. *Proc Natl Acad Sci U S A*. 2005;102(42):15030–15035.
7. Davydov IV, Varshavsky A. RGS4 is arginylated and degraded by the N-end rule pathway in vitro. *J Biol Chem*. 2000;275(30):22931–22941.
8. Hu RG, et al. The N-end rule pathway as a nitric oxide sensor controlling the levels of multiple regulators. *Nature*. 2005;437(7061):981–986.
9. Berman DM, Gilman AG. Mammalian RGS proteins: barbarians at the gate. *J Biol Chem*. 1998; 273(3):1269–1272.
10. De Vries L, Zheng B, Fischer T, Elenko E, Farquhar MG. The regulator of G protein signaling family. *Annu Rev Pharmacol Toxicol*. 2000;40:235–271.
11. Lambert NA, et al. Regulators of G-protein signaling accelerate GPCR signaling kinetics and govern sensitivity solely by accelerating GTPase activity. *Proc Natl Acad Sci U S A*. 2010;107(15):7066–7071.
12. Hubbard KB, Hepler JR. Cell signalling diversity of the Gqalpha family of heterotrimeric G proteins. *Cell Signal*. 2006;18(2):135–150.
13. Tirziu D, Simons M. Endothelium-driven myocardial growth or nitric oxide at the crossroads. *Trends Cardiovasc Med*. 2008;18(8):299–305.
14. Sugden PH, Clerk A. Regulation of the ERK subgroup of MAP kinase cascades through G protein-coupled receptors. *Cell Signal*. 1997;9(5):337–351.
15. van Berlo JH, Maillet M, Molkentin JD. Signaling effectors underlying pathologic growth and remodeling of the heart. *J Clin Invest*. 2013;123(1):37–45.
16. Dupre DJ, Robitaille M, Rebois RV, Hebert TE. The role of Gbetagamma subunits in the organization, assembly, and function of GPCR signaling complexes. *Annu Rev Pharmacol Toxicol*. 2009;49:31–56.
17. Kerchner KR, et al. Differential sensitivity of phosphatidylinositol 3-kinase p110gamma to isoforms of G protein betagamma dimers. *J Biol Chem*. 2004;

279(43):44554–44562.
18. Naga Prasad SV, Esposito G, Mao L, Koch WJ, Rockman HA. Gbetagamma-dependent phosphoinositide 3-kinase activation in hearts with in vivo pressure overload hypertrophy. *J Biol Chem*. 2000; 275(7):4693–4698.
19. Ma XMBlenis J. Molecular mechanisms of mTOR-mediated translational control. *Nat Rev Mol Cell Biol*. 2009;10(5):307–318.
20. Autiero M, et al. Role of PlGF in the intra- and intermolecular cross talk between the VEGF receptors Flt1 and Flk1. *Nat Med*. 2003;9(7):936–943.
21. Carmeliet P, et al. Synergism between vascular endothelial growth factor and placental growth factor contributes to angiogenesis and plasma extravasation in pathological conditions. *Nat Med*. 2001;7(5):575–583.
22. Li W, et al. High-resolution quantitative computed tomography demonstrating selective enhancement of medium-size collaterals by placental growth factor-1 in the mouse ischemic hindlimb. *Circulation*. 2006;113(20):2445–2453.
23. Luttun A, et al. Revascularization of ischemic tissues by PlGF treatment, and inhibition of tumor angiogenesis, arthritis and atherosclerosis by anti-Flt1. *Nat Med*. 2002;8(8):831–840.
24. Roncal C, et al. Beneficial effects of prolonged systemic administration of PlGF on late outcome of post-ischaemic myocardial performance. *J Pathol*. 2008;216(2):236–244.
25. Accornero F, et al. Placental growth factor regulates cardiac adaptation and hypertrophy through a paracrine mechanism. *Circ Res*. 2011;109(3):272–280.
26. Ni YG, et al. Foxo transcription factors blunt cardiac hypertrophy by inhibiting calcineurin signaling. *Circulation*. 2006;114(11):1159–1168.
27. Rengo G, et al. Myocardial adeno-associated virus serotype 6-betaARKct gene therapy improves cardiac function and normalizes the neurohormonal axis in chronic heart failure. *Circulation*. 2009; 119(1):89–98.
28. Camps M, et al. Blockade of PI3Kgamma suppresses joint inflammation and damage in mouse models of rheumatoid arthritis. *Nat Med*. 2005; 11(9):936–943.
29. Wang C, Jayadev S, Escobedo JA. Identification of a domain in the angiotensin II type 1 receptor determining Gq coupling by the use of receptor chimeras. *J Biol Chem*. 1995;270(28):16677–16682.
30. Molkentin JD, et al. A calcineurin-dependent transcriptional pathway for cardiac hypertrophy. *Cell*. 1998;93(2):215–228.
31. Lunde IG, Kvaloy H, Austbo B, Christensen G, Carlson CR. Angiotensin II and norepinephrine activate specific calcineurin-dependent NFAT transcription factor isoforms in cardiomyocytes. *J Appl Physiol*. 2011;111(5):1278–1289.
32. Furfine ES, et al. Potent and selective inhibition of human nitric oxide synthases. Selective inhibition of neuronal nitric oxide synthase by S-methyl-L-thiocitrulline and S-ethyl-L-thiocitrulline. *J Biol Chem*. 1994;269(43):26677–26683.
33. Flaherty MP, et al. eNOS deficient mice develop progressive cardiac hypertrophy with altered cytokine and calcium handling protein expression. *Cardiovasc Toxicol*. 2007;7(3):165–177.
34. Tomanek RJ, Busch TL. Coordinated capillary and myocardial growth in response to thyroxine treatment. *Anat Rec*. 1998;251(1):44–49.
35. Gaasch WH. Left ventricular radius to wall thickness ratio. *Am J Cardiol*. 1979;43(6):1189–1194.
36. Sugishita Y, Koseki S, Matsuda M, Yamaguchi T, Ito I. Myocardial mechanics of athletic hearts in comparison with diseased hearts. *Am Heart J*. 1983;105(2):273–280.
37. Weiner RB, Baggish AL. Exercise-induced cardiac remodeling. *Prog Cardiovasc Dis*. 2012;54(5):380–386.
38. Walsh K, Shiojima I. Cardiac growth and angiogenesis coordinated by intertissue interactions. *J Clin Invest*. 2007;117(11):3176–3179.
39. Guo Y, et al. Genetic background, gender, age, body temperature, and arterial blood pH have a major impact on myocardial infarct size in the mouse and need to be carefully measured and/or taken into account: results of a comprehensive analysis of determinants of infarct size in 1,074 mice. *Basic Res Cardiol*. 2012;107(5):288.
40. Bry M, et al. Vascular endothelial growth factor-B acts as a coronary growth factor in transgenic rats without inducing angiogenesis, vascular leak, or inflammation. *Circulation*. 2010;122(17):1725–1733.
41. Barouch LA, et al. Nitric oxide regulates the heart by spatial confinement of nitric oxide synthase isoforms. *Nature*. 2002;416(6878):337–339.
42. Balligand JL, Feron O, Dessy C. eNOS activation by physical forces: from short-term regulation of contraction to chronic remodeling of cardiovascular tissues. *Physiol Rev*. 2009;89(2):481–534.
43. Ahmad S, et al. Direct evidence for endothelial vascular endothelial growth factor receptor-1 function in nitric oxide-mediated angiogenesis. *Circ Res*. 2006;99(7):715–722.
44. Tesmer VM, Kawano T, Shankaranarayanan A, Kozasa T, Tesmer JJ. Snapshot of activated G proteins at the membrane: the Galphaq-GRK2-Gbetagamma complex. *Science*. 2005;310(5754):1686–1690.
45. Zhong H, et al. A spatial focusing model for G protein signals. Regulator of G protein signaling (RGS) protien-mediated kinetic scaffolding. *J Biol Chem*. 2003;278(9):7278–7284.
46. Takimoto E, et al. Regulator of G protein signaling 2 mediates cardiac compensation to pressure overload and antihypertrophic effects of PDE5 inhibition in mice. *J Clin Invest*. 2009;119(2):408–420.
47. Tamirisa P, Blumer KJ, Muslin AJ. RGS4 inhibits G-protein signaling in cardiomyocytes. *Circulation*. 1999;99(3):441–447.
48. Tokudome T, et al. Regulator of G-protein signaling subtype 4 mediates antihypertrophic effect of locally secreted natriuretic peptides in the heart. *Circulation*. 2008;117(18):2329–2339.
49. Rogers JH, et al. RGS4 causes increased mortality and reduced cardiac hypertrophy in response to pressure overload. *J Clin Invest*. 1999;104(5):567–576.
50. Rogers JH, et al. RGS4 reduces contractile dysfunction and hypertrophic gene induction in Galpha q overexpressing mice. *J Mol Cell Cardiol*. 2001; 33(2):209–218.
51. D'Angelo DD, et al. Transgenic Galphaq overexpression induces cardiac contractile failure in mice. *Proc Natl Acad Sci U S A*. 1997;94(15):8121–8126.
52. Mende U, et al. Transient cardiac expression of constitutively active Galphaq leads to hypertrophy and dilated cardiomyopathy by calcineurin-dependent and independent pathways. *Proc Natl Acad Sci U S A*. 1998;95(23):13893–13898.
53. Xie Y, et al. Breast cancer migration and invasion depend on proteasome degradation of regulator of G-protein signaling 4. *Cancer Res*. 2009; 69(14):5743–5751.
54. Kirui JK, et al. Gbetagamma signaling promotes breast cancer cell migration and invasion. *J Pharmacol Exp Ther*. 2010;333(2):393–403.
55. Hamed EA, Zakhary MM, Maximous DW. Apoptosis, angiogenesis, inflammation, and oxidative stress: basic interactions in patients with early and metastatic breast cancer. *J Cancer Res Clin Oncol*. 2012;138(6):999–1009.
56. Sjogren B, Neubig RR. Thinking outside of the "RGS box": new approaches to therapeutic targeting of regulators of G protein signaling. *Mol Pharmacol*. 2010;78(4):550–557.
57. Tsai EJ, Kass DA. Cyclic GMP signaling in cardiovascular pathophysiology and therapeutics. *Pharmacol Ther*. 2009;122(3):216–238.
58. Fiedler B, et al. Inhibition of calcineurin-NFAT hypertrophy signaling by cGMP-dependent protein kinase type I in cardiac myocytes. *Proc Natl Acad Sci U S A*. 2002;99(17):11363–11368.
59. Fiedler B, Wollert KC. Interference of antihypertrophic molecules and signaling pathways with the Ca2+-calcineurin-NFAT cascade in cardiac myocytes. *Cardiovasc Res*. 2004;63(3):450–457.
60. Koitabashi N, et al. Cyclic GMP/PKG-dependent inhibition of TRPC6 channel activity and expression negatively regulates cardiomyocyte NFAT activation Novel mechanism of cardiac stress modulation by PDE5 inhibition. *J Mol Cell Cardiol*. 2010; 48(4):713–724.
61. Wilkins BJ, et al. Calcineurin/NFAT coupling participates in pathological, but not physiological, cardiac hypertrophy. *Circ Res*. 2004;94(1):110–118.
62. DiPalma T, et al. The placenta growth factor gene of the mouse. *Mamm Genome*. 1996;7(1):6–12.
63. Chang B, Mathew R, Palmer LS, Valderrama E, Trachtman H. Nitric oxide in obstructive uropathy: role of endothelial nitric oxide synthase. *J Urol*. 2002;168(4 Pt 2):1801–1804.
64. Kemuriyama T, et al. Endogenous angiotensin II has fewer effects but neuronal nitric oxide synthase has excitatory effects on renal sympathetic nerve activity in salt-sensitive hypertension-induced heart failure. *J Physiol Sci*. 2009;59(4):275–281.
65. Komers R, Lindsley JN, Oyama TT, Anderson S. Effects of long-term inhibition of neuronal nitric oxide synthase (NOS1) in uninephrectomized diabetic rats. *Nitric Oxide*. 2004;11(2):147–155.
66. Graveleau C, et al. Mouse and human resistins impair glucose transport in primary mouse cardiomyocytes, and oligomerization is required for this biological action. *J Biol Chem*. 2005; 280(36):31679–31685.
67. Tang M, et al. Proteasome functional insufficiency activates the calcineurin-NFAT pathway in cardiomyocytes and promotes maladaptive remodelling of stressed mouse hearts. *Cardiovasc Res*. 2010; 88(3):424–433.
68. Zagorchev L, et al. Micro computed tomography for vascular exploration. *J Angiogenes Res*. 2010;2:7.
69. Jiang Y, Zhuang Z, Sinusas AJ, Papademetris X. Vascular tree reconstruction by minimizing a physiological functional cost. *Conf Comput Vis Pattern Recognit Workshops*. 2010;178–185.
70. Frangi A, Niessen W, Vincken K, Viergever M. Multiscale vessel enhancement filtering. In: Wells W, Colchester A, Delp S, eds. *Medical Image Computing and Computer-Assisted Interventation 1998*. Berlin, Germany: Springer Berlin; 1998:130–137.
71. Lee TC, Kashyap RL, Chu CN. Building skeleton models via 3-D medial surface axis thinning algorithms. *CVGIP: Graphical Models and Image Processing*. 1994;56(6):462–478.
72. Murray CD. The physiological principle of minimum work: I. The vascular system and the cost of blood volume. *Proc Natl Acad Sci U S A*. 1926; 12(3):207–214.